Estuarine, Coastal and Shelf Science (1999) **48,** 307–324
Article No. ecss.1998·0422, available online at http://www.idealibrary.com on IDEAL

The Propagation of Tides up Rivers With Special Considerations on the Upper Saint Lawrence River

G. Godin

301 Hinchey ave, Ottawa Ont, Canada K1Y 1M1

Received 4 May 1998 and accepted 17 September 1998

The hydrodynamics of rivers affected by tides is dominated by the damping and the distortion induced by quadratic bottom friction. A compact and accurate approximation to the deceleration term, standing for the frictional effect, allows the retention of the concept of harmonics and separation of the time and space variations. It then becomes possible to explain, in terms of basic physics, the transformation of the tide from the estuary, to the zone where it becomes extinct. The theoretical reasoning is supported by pertinent observations collected in the Saint Lawrence river; numerical relations are derived to demonstrate the existence of non-linear effects and to quantitatively link various relevant physical parameters. This analysis, in turn, helps outline approaches to improve the tide predictions in such rivers which happen to have such great economic and strategic importance.

Keywords: tides; wave propagation; rivers; fresh water outflow; Saint Lawrence river

Introduction

The tide entering into rivers behaves as a wave progressing upstream, increasingly distorted and eventually extinguished by bottom friction. The latter is proportional to the square of the velocity, integrated over the vertical, of the instantaneous current, thus introducing a non-linearity in the equation for momentum balance. The physical effects of quadratic friction, besides requiring difficult mathematics for discerning them, frequently escape (and even go against) our intuition. It also happens that rivers where tides exist serve as important economic feeders to the hinterland so practical information about their tides and currents is, therefore, necessary. Tide tables routinely provide predictions for harbours sited in rivers. A close look shows them to be rather unsatisfactory because of extraneous factors of minor importance in the open ocean but dominant in rivers, which affect the incoming wave. In what follows we shall review what actually occurs in tided rivers, using for this purpose data collected in the Saint Lawrence river (Figure 1). This river has a near perfect physical configuration, suffers no major problems of silting and provides an abundance of data which was collected at strategic points during the 1960's and 1970's. Conversely, the results obtained from mathematical developments and the hard information gathered from the Saint Lawrence, apply to all rivers emptying into the ocean.

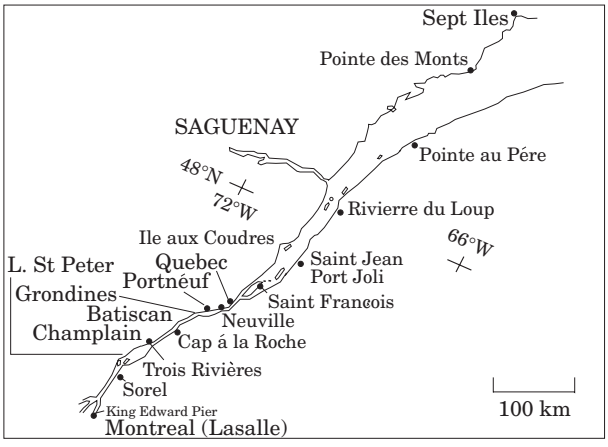

FIGURE 1. Upper Saint Lawrence river along which are shown most of the sites mentioned in the paper.

Bottom friction

Bottom friction is described by the deceleration term containing u|u|, in Newton's equation of motion for fluids in a canal:

$$\frac{\partial u}{\partial t}+u\frac{\partial u}{\partial x}=-g\frac{\partial Z}{\partial x}-\frac{\mu u|u|}{H+Z} \qquad (1)$$

u=current (m/s) (made up of $-u_o(x)+u(x,t)$, the contributions of the fresh water outflow and of the incoming tidal wave)
Z=surface displacement (m)

0272–7714/99/030307+18 $30.00/0

t = time
x = distance (km)
H(x) = mean depth (m)
μ = coefficient of friction (dimensionless $\approx 3 \times 10^{-3}$).

The acting force is the horizontal pressure gradient $g\partial Z/\partial x$. Orders of magnitude for the surface slope $\partial Z/\partial x$ prevailing in the Saint Lawrence river are the following:

(a) due to u_o: 5·5–7·9 m between Montréal and Québec (Godin, 1971) or $2{\cdot}4–3{\cdot}4 \times 10^{-2}$/km, the larger gradients prevailing during the winter months

(b) due to the tide: between Ile aux Coudres and Batiscan, the phase difference is about 180° so that the local levels oscillate in opposite directions (Godin, 1981). The level difference contributed by the tide amounts to 2–3 m or $1{\cdot}4–2{\cdot}1 \times 10^{-2}$/km

(c) due to wind stress: according to Ekman (1953) it is given by:

$$\frac{\partial Z}{\partial x} = \frac{3}{2}\frac{\tau}{g\rho H} \quad \text{where} \quad \tau = 2{\cdot}6 \times 10^{-3}\rho' w^2$$

ρ' is the density of the air, ρ that of the water, w is the wind speed. For a wind speed of 17 m/s (60 km/h), the added slope amounts to $0{\cdot}7 \times 10^{-2}$/km

(d) due to barometric pressure gradients: a pressure difference of 10 mb between two points adds an additional 10 cm to the slope

(e) due to the ice stress: the formation of ice introduces gradients whose effect is immediately apparent in tidal records. It is not possible however to offer any meaningful estimates.

The pressure gradient is balanced by the outflow of fresh water and by the incoming tidal wave if we disregard the other transient contributions. The fresh water discharge is defined by:

$$Q = W(x)H(x)\, u_o(x) \text{ m}^3/\text{sec}$$

W(x) = width(m) of the river at point x and we assume that Q originates exclusively from upstream. Q is monitored at Lasalle for the Saint Lawrence.

Both contributors to u are time dependent but the time scales of their variability differ widely, one in terms of days or weeks, the other changing hourly. This feature allows seeking an explicit solution of Equations (1) and (13), which is given by the expressions (16) and (17). u|u| is a non-linearity which can be handled analytically when we note that as an odd function, it is expressable as $Au+Bu^3$ or $Au+Bu^3+Cu^5$ etc, once the physical dimension of u is removed, A, B and C being suitable constants (Doodson, 1924, 1956; Godin, 1991*a*,*b*). In what follows we shall use the expression:

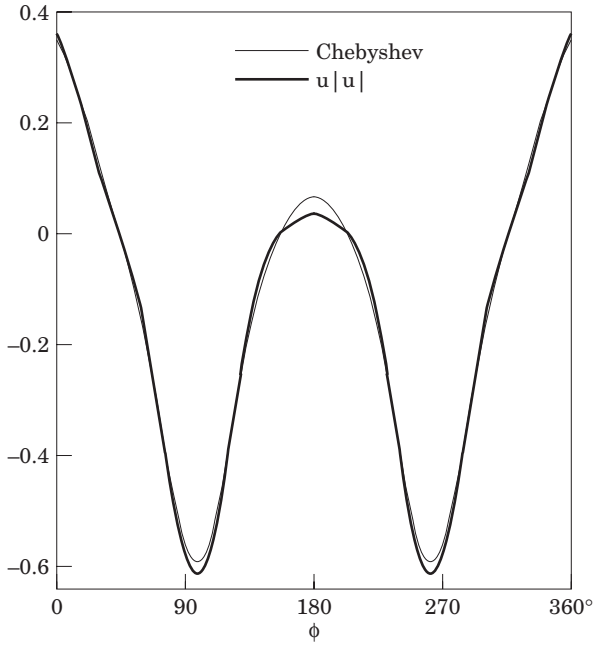

FIGURE 2. Approximation to u|u| by Chebyshev polynomials, this type of approximation removes the need for series expansions to deal with this non-linearity. [u = −0·2+ 0·2 cosφ+0·6 cos 2φ].

$$u(x,t)|u(x,t)| \approx U(x)^2[0{\cdot}3395u'(x,t) + 0{\cdot}6791u'(x,t)^3] \qquad (2)$$

where:

$$U(x) \equiv \Sigma_{j=1}^{n} u_j(x) \quad u'(x,t) = \Sigma_{j=1}^{n} a_j \cos[\sigma_j t - b_j(x)]$$
$$a_j \equiv u_j(x)/U(x)$$

U = maximum possible value of the current at point x
u_j = amplitude of the current component of frequency σ_j at x
a_j = dimensionless variable satisfying $a_j < 1$, $\Sigma_j a_j = 1$. The numerical coefficients arise from using Chebyshev polynomials (Lanczos, 1956) to approximate u|u|, since they guarantee the least maximum absolute error. As demonstrated in Figure 2, the approximation to a typical river current is surprisingly accurate.

Concepts to be abandoned

Since quadratic friction creates a non-linear distortion of the signal, we must be ready to abandon some of the concepts associated with wave motion if we wish to fully understand the phenomenon of tidal propagation up rivers.

1. *The coefficient of friction* μ

Engineering manuals supply values of μ for canals of various structures. The moment the current starts

oscillating, μ in fact, becomes impossible to assess. The damping now depends not only on μ, given a type of bottom, but also on $U^2(x)$ and on the mix of harmonics present. U(x) will vary with each set of harmonics introduced and their relative amplitudes. As the current shifts from large to small intensities over the tidal cycles, the frictional characteristics of the channel will vary continuously. The addition of a net current due to the fresh water discharge will also alter the type of non-linear interactions occurring (see below: ' Character of the damping '). If the canal is long enough, the internal structure of the signal upstream will vary from point to point, so that the local frictional distortion will acquire its own character, yet in a fixed and unchanging canal whose bottom rugosity and perforce remains invariant. We must therefore resign ourselves to only vague estimates of μ. (In the practice of numerical modelling, the correct μ is the one which gives the best overall fit; if in addition to M_2, one also tries to model S_2 and K_1, it will soon be concluded that different values of μ become necessary).

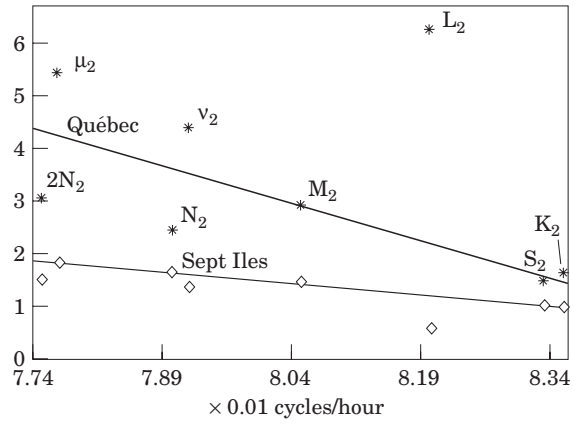

FIGURE 3. Response diagrams for Sept Iles (lozenges) and Québec (stars), plotted is the ratio between the amplitude of the harmonic at the site and its ' equilibrium amplitude ' (theoretical). The frequency of the harmonic is plotted on the horizontal scale.

2. *Harmonic ' constants '*

A set of harmonics $u_j(x,t)$ was introduced in the previous expressions, this being the classical method to initiate the study of non-linear effects, it allows the solving of the equations of hydrodynamics by successive approximations. The scrutiny of the u|u| non-linearity that concerns us will show that we can seek solutions in terms of harmonics even in its presence but that they cannot be constants. A harmonic ' constant ' is a sinusoid whose amplitude and phase lag are invariant at a given point. The concept, introduced by Laplace (1841), was applied to the tide in oceans and proved successful. If the signal progresses from elsewhere into a river, the constancy becomes impossible to sustain in the presence of quadratic friction. The tidal harmonics are packed very tightly on the frequency scale; their interference cycles consequently have periodicities of weeks or months. The resultant will therefore be damped at different rates as time elapses: we illustrate this in Figure 3. This shows response diagrams for two stations in the Saint Lawrence, Sept Iles located downstream and Québec, where the channel narrows. A response diagram gives the ratio between the amplitude of the harmonic at the site and its equilibrium amplitude. At Sept Iles (lower curve) the sample points follow a linear trend, with the exception of the minor harmonics which stray only slightly. At Québec (upper curve), the frequencies which lie very close to each other appear on opposite sides of the curve. What Figure 3 means to represent is physically impossible, an extended and uniform medium such as the ocean cannot respond in such wildly disparate fashion to harmonics separated by barely 0·001 c/h. The estimates given by the spectral analysis are wrong, the reason being that the spectral elements are not independent of each other. The essential mathematical prerequisite for obtaining a meaningful spectrum consisting of independent estimates for each frequency, is that the process must be linear (Jenkins & Watts, 1968), most oceanographic processses contain some non-linearities, tides being one example. Non-linearities become severe in rivers and in many estuaries. This is illustrated further in Figures 4 and 5. Figure 4 depicts the amplitude of the admittance $A(\sigma)$, defined by:

$$A_{xy}(\sigma) = \frac{Z_{xy}(\sigma)}{Z_x(\sigma)} \qquad (3)$$

$Z_{xy}(\sigma)$ is the cross spectrum between two time sequences {x(t)} and {(y(t)}, $Z_x(\sigma)$ being the power spectrum of the input sequence {(x(t)}; this results in the admittance being a complex number with amplitude and phase (Bendat & Piersol, 1966). Treating the tide at Sept Iles as input and the one at Québec as output, Figure 4 provides spectral samples over intervals of 48 h (adequate to provide a band resolution) over the same semi-diurnal band. Plotted below, as a relevant parameter, is the value of the highest level reached at the input (Sept Iles) over the two days, and reflects the cycles between large and small tides (spring and neap). The admittance amplitude and phase should be constant for a linear process: the measured admittance amplitude in fact oscillates between 1·5 and 2·5 around a mean value of 2, its peaks

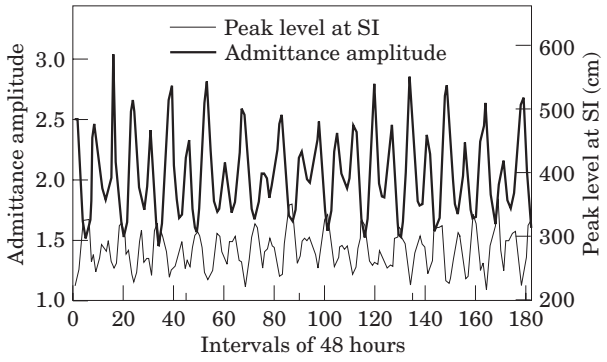

FIGURE 4. Amplitude of the admittance between Québec and Sept Iles in the semi-diurnal band for 1974. This reflects the ratio between the amplitude of the harmonic at Québec (output) and its amplitude at Sept Iles (input). The finer line gives the maximum level (right hand scale) reached at the input over one tidal cycle, reflecting the range of the tide at the entrance of the river, a measure of its energy. The admittance amplitude makes it clear that the more energetic tides suffer more frictional damping on their way to Québec.

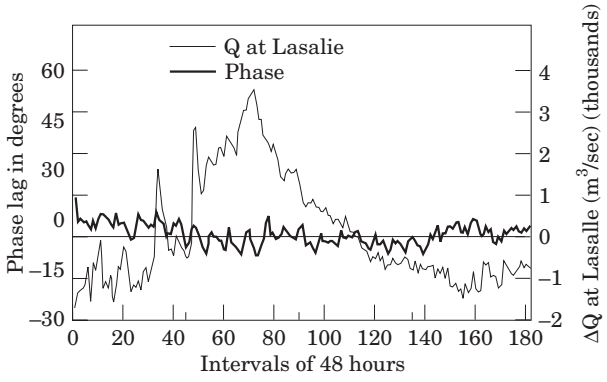

(Québec with a lag of 5 hours)

FIGURE 5. The phase of the admittance measures the time it takes the wave to reach Québec from Sept Iles. The finer curve in the background is the fresh water discharge Q, measured at Montréal (deviation from its mean annual value, right hand scale). A weak correlation exists between the time it takes the oceanic tide to reach Québec and the volume of the discharge.

and valleys being negatively correlated with the tidal cycles at Sept Iles. Annual analyses give 91 and 183 cm for the M_2 tide at the two stations; they thus reflect the mean value of the admittance amplitude equivalent to the ratio 2:1. Figure 4 shows that the M_2 tide at Québec may in fact be larger or smaller than 183 cm. The varying admittance amplitudes are consistent with the effects of quadratic friction, the stronger tides downstream are more strongly damped than the weaker tides when they travel upstream. A smaller admittance amplitude, however, does not mean that large tides at Sept Iles reach Québec as

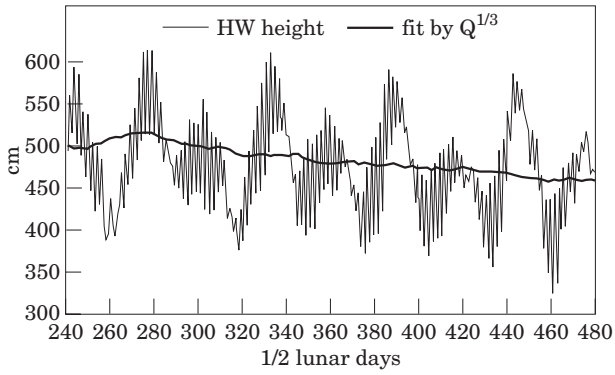

FIGURE 6. HW height profile at Québec, this differs little from the profile of HW measured around the rim of the open oceans.

small tides, but rather that they are not as strong there as if they had been propagated linearly.

The phase of the admittance (Figure 5), conversely, shows it to be remarkably regular, the time of the wave's arrival at Québec varying by, at most, a few minutes. The natural logarithm of 2·5/1·5 is 0·51 radians or 29° when expressed in degrees, implying fluctuations of $\pm 15°$; what is observed is $\pm 5°$. The discrepancy between the damping and the dephasing is attributed to the crest of High Water (HW) travelling faster than the trough of Low Water (LW), resulting in approximately constant times for the arrival of the mean wave. The slight ripples in the phase do not correlate with the range of the tide downstream but they do so, albeit very slightly, with the variations in the intensity of the flow of fresh water emerging from the Great Lakes (in the background). The deviation of the daily discharge Q was plotted from its mean annual value. The character of the ripples also appears to differ slightly between intervals of increasing or decreasing discharge.

Irregularities in the height and time of high and low water at Québec

Figures 6 and 7 show the profiles of HW and LW at the site; the time interval covers 5 May to 7 September 1974, during which the local level was affected by a peak in the discharge occurring after the snow meltdown. As oscillations they differ markedly; HW behaves as a conventional tide, the jagged fluctuations reflecting the diurnal inequality, while the profile of LW, which should be almost identical, shows much more irregularity. As will be observed later, HW at the site presents no special difficulty while biases appear in comparisons between the observed and predicted LW. The trend with time in

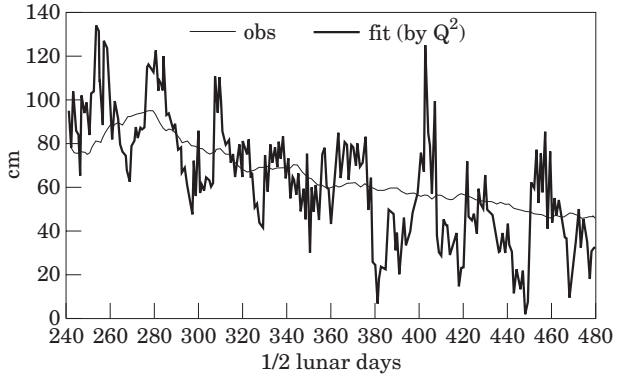

FIGURE 7. Profile of LW at the very same site, this is much more irregular. The fit with the discharge Q helps to control some of the variation.

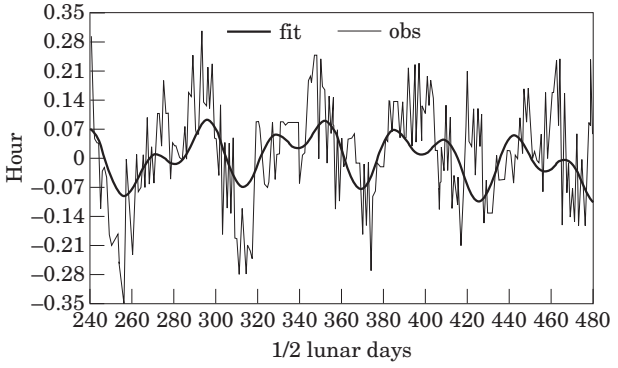

FIGURE 8. Time error on HW at Québec, the difference between the actual time of occurrence and the prediction. The drift in the reference level due to Q, apparent in the previous figure, has been removed using the fit by the harmonics Mm and MSf. Long period harmonic variations are now apparent.

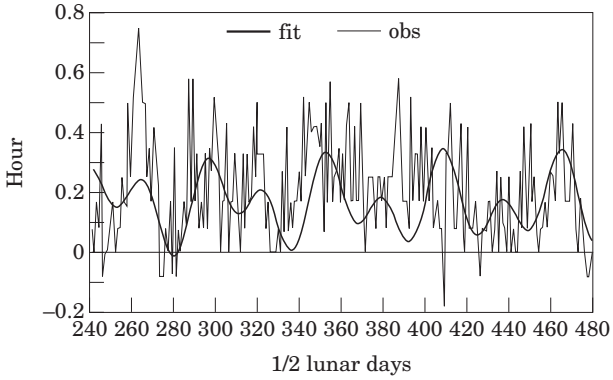

Fit by Zo Mm MSf(Mf)

FIGURE 9. Error on the predicted time of LW at Québec.

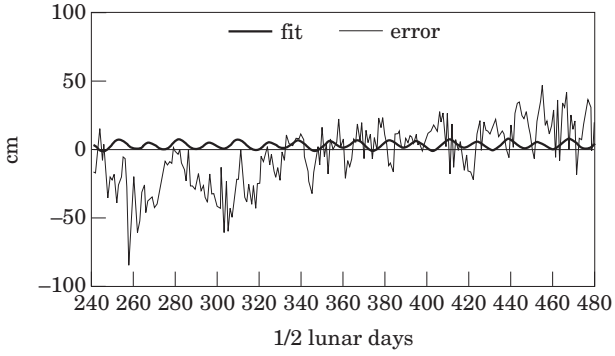

FIGURE 10. Error on the height of HW at Québec.

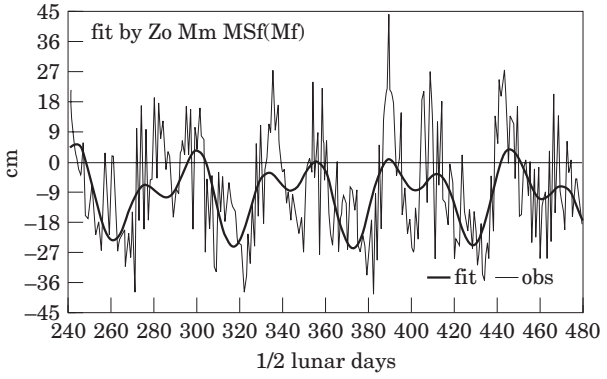

FIGURE 11. Error on the height of LW at Québec, the long period modulations are more marked than for HW.

the mean level may be adjusted by fitting with the value of the fresh water discharge, Q, measured at Lasalle, Montréal (the fit was applied to all the data for the year). The power to which Q must be raised for an acceptable fit is less for the height of HW than for that of LW (0·333←→2·000); physically this means that the height of HW is not as sensitive to Q as that of LW. Figures 8 and 9 give the time error for LW and HW after the effect of Q has been removed (slight but detectable). The time error is the difference between the observed time and that derived from conventional harmonic predictions. In addition to the influence of Q and the presence of obvious modulations (previously noticed by Doodson, 1957), biases are noticeable, especially at LW. The periodicities (extracted from the data for the whole year) have periods of 15 and 28 days, corresponding with the interference cycles of M_2 and S_2 (14·8 days), M_2 and N_2 (27·6 days), thus making obvious the presence of quadratic friction. Figures 10 and 11 show the errors in the predicted heights once the effect of Q has been removed. The purging of Q seems to have failed for the HW, but since the $Q^{1/3}$ fit stabilized the error over the remaining year, it was retained. Placed in perspective, the errors in the predicted heights of HW and their periodicities are smaller than those affecting LW.

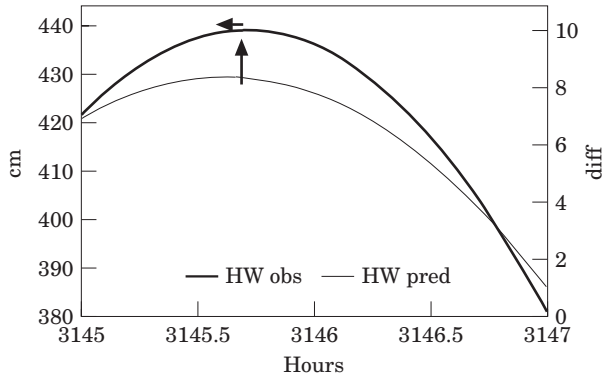

FIGURE 12. Close up view of the observed and predicted curve near HW on 11 May 1977. The thicker curve is the actual observation. HW tends to occur ahead of the predicted time and is higher than the level predicted.

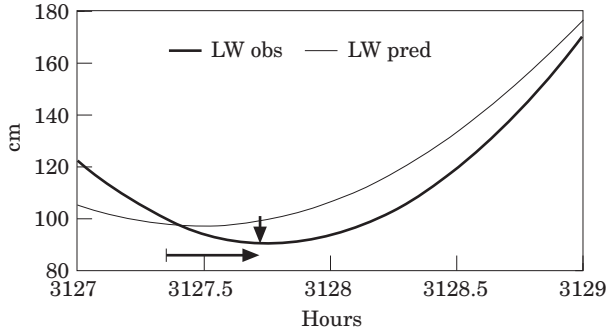

FIGURE 13. Close up view of the observed and predicted curve near LW. LW is lower and later than predicted.

The results indicate that LW occurs later and is lower than predicted, while HW occurs slightly earlier and is higher than predicted. This behaviour is depicted with more details in Figures 12 and 13. The hourly observations were interpolated over 12 segments of five minutes using Lagrange coefficients; the predictions were generated over the same intervals. May 10–11 coincides with a subsidence in the flow of fresh water which had peaked during March–April, Q amounted to 9700–9800 m^3/s during the interval. The predicted HW misses the high from below, differing only slightly in its timing; the predicted LW misses the low from above and is definitely too early. In the reality of records, everything is possible but the most common occurrences are those illustrated. This is upheld by statistics on the errors.

A closer look at the friction term

We return to Equation (1) in an attempt to relate the distortions just noted in a river tide, with the existence of frictional deceleration. What was observed at Québec is what occurs upstream of a given point in all rivers affected by tides; on some rare occasions a bore may also be generated in the same area. As stated previously, the friction term overwhelms the other terms in the equation of motion. First the convective term $u\partial u/\partial x$ may be dismissed as negligible. Considering a current of magnitude 1 m/s in a river 5 m in depth where the tide has a range of 1 m, which becomes extinguished over a distance of 10 km (an extreme case), we find:

$$u\frac{\partial u}{\partial x} = 1 \times \frac{1}{10\,000} = 1 \times 10^{-4}\ \mathrm{m/s^2} \qquad (4)$$

$$\mu\frac{u|u|}{H+Z} = \frac{3 \times 10^{-3}}{4 \to 6} \geq 5 \times 10^{-4}\ \mathrm{m/s^2} \qquad (5)$$

$\partial u/\partial t$ has magnitude $1{\cdot}4 \times 10^{-4}\ m/s^2$ for a semi-diurnal tide while the horizontal pressure gradient maintains the remainder of the momentum balance. Shallow water effects created by the presence of Z in the denominator of the friction term have an effect of some ± 20%. We therefore concentrate on the inspection of the $u|u|$ term before seeking solutions to the equations of hydrodynamics when it is present. The term was approximated as $(u|u|)/U^2(x) \approx Au + Bu^3$. Using a set of harmonics as a linearized input, this requires taking the cube of a sum of harmonics, in addition to their linear superposition. Mathematically, the cubing of trigonometric functions creates linear combinations of sets of three of the incoming harmonics; physically such combinations are viewed as ‘ triple interactions ’. Although the bottom friction term is quadratic, it always results in the interactions of three, not two, harmonics. We could always seek a closer approximation, such as $Au + Bu^3 + Cu^5$; in this case Chebyshev polynomials provide A=0·2183, B=1·1641 and C= − 0·3880. The optimum constants A, B and C for the improved fit differ completely from those used previously; they would be the same in a conventional series development (Pingree, 1983). Numerical approximations, such as those presented here, not only keep the set of equations to be solved closed, but become the only approach possible when more than two harmonics need to be considered (See Appendix in Godin & Martinez, 1994). The worst possible error on a normalized u is now 0·013 or 1·3%, while the average error is 0·006. This approximation leads to additional fifth order interactions, any set of five of the incoming harmonics interfering with each other. The scrutiny of tidal records shows that interactions of order ranging from 2–10 are detectable; since our approximation is almost perfect for 5, the higher order interactions occur when we pursue

TABLE 1. Development of $u|u|/U^2$ by the approximation $Au+Bu^3$

$\sigma=0$	$\leftarrow\rightarrow$	$-a_o\left[A+B\left(a_o^2+\frac{3}{2}\Sigma_j a_j\right)\right]$
$\cos[\sigma_j t-b_j(x)]$	$\leftarrow\rightarrow$	$\left(A+B\left(3a_o^2+\frac{3}{4}a_j^2+\frac{3}{2}\Sigma_{k\neq j}a_k^2\right)\right)a_j$
$\cos[2(\sigma_j t-b_j(x)]$	$\leftarrow\rightarrow$	$-\frac{3}{2}Ba_o a_j^2$
$\cos[3(\sigma_j t-b(x)]$	$\leftarrow\rightarrow$	$\frac{B}{4}a_j^3$
$\cos[\sigma_j\pm\sigma_k)t-(b_j(x)\pm b_k(x))]$	$\leftarrow\rightarrow$	$-3Ba_o\Sigma_{k\neq j}a_j a_k$
$\cos[(2\sigma_j\pm\sigma_k)t-(2b_j(x)\pm b_j(x))]$	$\leftarrow\rightarrow$	$\frac{3}{4}B\Sigma_{k\neq j}a_k a_j^2$
$\cos[(\sigma_j\pm\sigma_k\pm\sigma_n)t-(b_j(x)\pm b_k(x)\pm b_n(x))]$	$\leftarrow\rightarrow$	$\frac{3}{2}B\Sigma_{j\neq k\neq n}a_j a_k a_n$

the solution of the basic equations a step further, moving from a first order to a second order solution.

Note that the outward current u_o created by the fresh water discharge Q behaves as a harmonic of frequency 0; it eventually becomes dominant as the wave progresses upstream. We display in Table 1 the algebraic development of the time dependent portion of u|u|, where:

$$u(x,t) = -u_o(x)+\Sigma_{j=1}^{n}u_j(x)\cos[\sigma_j t-b_j(x)]$$
$$\equiv U(x)\,[-a_o(x)+\Sigma_{j=1}^{n}a_j(x)\cos[\sigma_j t-b_j(x)]] \quad (6)$$

restricting it to a cubic approximation since this will suffice to evaluate the physical consequences of quadratic bottom friction on the propagation of tidal waves. In our co-ordinate convention, we took upstream as the direction of increasing x so that u_o and its associated parameter $a_o\equiv u_o/U$ carry a negative sign. The linear portion given by Au affects the original harmonics. Bu^3 also modifies these but creates new harmonics within the tidal band as well as in the upper and lower frequency bands. This is the root cause of all the phenomena so far encountered, and additional phenomena which will eventually become apparent. The development of u|u| reveals that we may continue to approach the problem of non-linear effects using the concept of harmonics. We also succeeded in keeping separate the time and space variations which normally become entangled in the presence of non-linearities. Thus, we gain immediate insights into the spectral transformations undergone by the tidal wave as it progresses upstream, even before solving the equations of hydrodynamics. We concentrate on the terms carrying the factor B, since they reveal features which completely escape our intuition. We note first that there are always three a values whenever we deal with B: this allows approximations dependent on their relative magnitudes and to predict *a priori*, without any further calculations, which of these are the most important interactions. In the development we encounter the original harmonics $(0,\{\sigma_j\})$ plus new ones:

(a) lower frequencies: $\sigma_j-\sigma_j=0$, $\sigma_j-\sigma_k$

(b) frequencies coinciding with or falling near the tidal frequencies:

$$2\sigma_j-\sigma_k,\ \sigma_j+\sigma_k-\sigma_n,\ \sigma_j-\sigma_k+\sigma_n$$

(c) higher frequencies: $2\sigma_j$, $\sigma_j+\sigma_k$, $\sigma_j+\sigma_k+\sigma_n$.

The higher frequencies emerge as M_4, MS_4, M_6 etc. Since some involve only two components, these could be assigned to shallow water effects or to the convective term. Since the latter is effectively negligible, the components arise from the frictional interaction of three components, one being the net current. The lower frequencies in the upper reaches of the river eventually exceed the magnitude of the tidal signal which manages to reach there and are therefore very important. The intermediate frequencies will superimpose themselves on harmonics such as L_2, μ_2, ν_2 and so on, making their response stray wildly from the common trend in the response diagram, as seen in Figure 3.

Self and mutual damping of the incoming tidal harmonics

Self and mutual damping can be evaluated from the term:

$$\left(A+B(3a_o^2+\frac{3}{4}a_j^2+\frac{3}{2}\Sigma_{k\neq j}a_k^2)\right)a_j \qquad (7)$$

The self damping is given by $A+3Ba_j^2/4$, the mutual damping arises from $B(3a_o^2+3\Sigma_{k\neq j}a_k^2/2)$. Up river where the tide weakens, the deceleration due to the fresh water outflow a_o dominates and will eventually force quadratic friction to behave linearly. In the intermediate zone, the tidal components will contribute to their own damping; the mutual damping is twice as large as the self damping. Consequently, the damping of a weak component is mainly controlled by its companions. Conversely, a major component such as M_2 will mostly feel its own damping and that of the outflow. It can be demonstrated (Godin 1991) that all of the small components are not extinguished completely by quadratic friction but are all damped at the same rate (larger than that of the dominant ones). The same formula shows that the moment an oscillatory current is superimposed on a steady flow, the intensity of friction is increased, since this term is four times as large as the self damping and twice as large as the mutual damping (always with a constant but quite unreachable μ).

The surface profile along the river

The surface profile is given by the first coefficient in Table 1:

$$-a_o\left[A+B(a_o^2+\frac{3}{2}\Sigma_j a_j^2)\right] \qquad (8)$$

When substituted in the equation of motion (1), the solution, since $\partial/\partial t=0$, consists of a negative gradient in the surface elevation. For $\{a_j\}=0$, we meet Chézy's law; in the zone where $\{a_j\}\neq 0$, the gradient is steepened by the present of tidal currents. The increased rise in elevation of the water surface has been successfully reproduced in a numerical model (Godin & Martinez, 1994).

Low and double frequencies

The low and double frequencies are $(\sigma_j-\sigma_k)$ and $2\sigma_j$ or $\sigma_j+\sigma_k$, these carry the coefficients:

$$-3Ba_o\Sigma_{k\neq j}a_j a_k \quad -\frac{3}{2}Ba_o a_j^2 \qquad (9)$$

The presence of a_o indicates that they cannot exist without a net outflow when friction predominates. They correspond to the compound harmonics $MS_o(M_2-S_2)=MSf$, $MN_o(M_2-N_2)=Mm$, $KO_o(K_1-O_1)=Mf$ or to M_4,MS_4,MN_4 and so on. As harmonics, the two classes of waves have different physical characteristics.

Character of the damping

We consider first the case of tides in the estuary where u_o is effectively negligible, restricting ourselves to a single harmonic. We denote the current as:

$$u_1(x,t)=A_1\cos(\sigma_1 t-a_1)$$

(The phase lags will be overlooked in what follows since they are not relevant to the discussion). Following the procedure outlined for formula (2): $U=A_1$ $a_1=1$ so that:

$$u|u|=A_1^2\cos\sigma_1 t|\cos\sigma_1 t|\approx A_1^2[A\cos\sigma_1 t + B\cos^3\sigma_1 t] \qquad (10)$$

We use:

$$\cos^3\alpha\equiv\frac{1}{4}(3\cos\alpha+\cos 3\alpha)$$

to obtain:

$$u|u|\approx A_1^2\left[\left(A+\frac{3}{B}\right)\cos\sigma_1 t+\frac{B}{4}\cos 3\sigma_1 t\right]$$
$$=A_1^2(0{\cdot}8488\cos\sigma_1 t+0{\cdot}1273\cos 3\sigma_1 t) \qquad (11)$$

The first factor coincides exactly with the $8/3\pi$ obtained in a Fourier development (practical only for a single component) of the $u|u|$ term, which can be encountered in textbooks on dynamical oceanography (for example see Proudman, 1953). Formula (10) tells us that in addition to damping effects, odd harmonics will also be generated in the area. We consider next a pair of harmonics:

$$u(x,t)=A_1(x)\cos\sigma_1 t+A_2(x)\cos\sigma_2 t$$

$U(x)=A_1+A_2$ $a_1=A_1/U$ $a_2=A_2/U$. We are faced with:

$$(a_1\cos\sigma_1 t+a_2\cos\sigma_2 t)^3=a_1^3\cos^3\sigma_1 t+a_2^3\cos^3\sigma_2 t + 3a_1^2a_2\cos^2\sigma_1 t\cos\sigma_2 t+3a_1a_2^2\cos\sigma_1 t\cos^2\sigma_2 t$$

This time not only triple harmonics are generated but also lower and higher harmonics: we forget about

these and concentrate on the original harmonics. After the algebra we obtain:

$$u|u| = U(x)\left(\left[A + B\left(\frac{3}{4}a_1^2 + \frac{3}{2}a_2^2\right)\right]A_1 \cos \sigma_1 t + \left[A + B\left(\frac{3}{4}a_2^2 + \frac{3}{2}a_1^2\right)\right]A_2 \cos \sigma_2 t + \ldots\right)$$

The effective friction coefficient is now $\mu U(x)$ times the numerical factor. If we take $A_1 = 0{\cdot}9$ $A_2 = 0{\cdot}1$ so that $U = 1$, we find that the factors for the two components are 0·7625 and 1·1714: the minor component becomes more damped. Had it travelled alone, it would have been damped according to the square of its amplitude and therefore much less that the major harmonic; accompanied by a larger companion, it now suffers even more than the leader of the pair.

We move next to the upper reaches of the river where the tide is nearing extinction. There, the oscillations occur around the position of equilibrium maintained by the discharge:

$$g\frac{\partial \zeta_o}{\partial x} = -\mu\frac{u_o^2}{H_o}$$

where we denote the position of the surface by $\zeta = \zeta_o + \zeta(x,t)$, the mean depth being H_o. The local current $u = -u_o + u(x,t)$. The second term denotes the tide, it being small enough that we may neglect products of $u(x,t)$ and $\zeta(x,t)$. The equation of continuity, W, being the width:

$$\frac{\partial(WHu)}{\partial x} = \frac{\partial(W\zeta)}{\partial t} \tag{12}$$

has a time varying portion:

$$-u_o\frac{\partial \zeta(x,t)}{\partial x} + H_o\frac{\partial u(x,t)}{\partial x} + \frac{\partial \zeta(x,t)}{\partial t} = 0 \tag{13}$$

assuming W = constant and H_o = constant. From now on we write $H \equiv H_o$ since everything occurs around this value. Similarly $u \equiv u(x,t)$ $\zeta \equiv \zeta(x,t)$ since these are the only variables of concern. Equation (1) becomes:

$$\left(\frac{\partial}{\partial t} + 2\mu\frac{u_o}{H}\right)u + g\frac{\partial \zeta}{\partial x} + \mu\frac{u_o^2\zeta}{H^2} - u_o\frac{\partial u}{\partial x} = 0 \tag{14}$$

The terms have been ordered in rank of importance, the first term shows the acceleration and the frictional effects, the second is the pressure gradient, the third represents the shallow water effect seen in the denominator of $u|u|$ in Equation (1) and the last is the convective term which is found to be negligible. Equations (13) and (14) emerge as linear, thus indicating that in the upper regions of a river, all the tidal components are damped uniformly by the outflow current $-u_o$: thus we can talk again of harmonic ' constants ' in that area. In principle we could retain all the terms in the explicit solution of (13) and (14); the resulting expressions turn out to be unwieldy due to the numerous terms they contain. We write out the explicit differential equation for ζ:

$$\left(g - \frac{u_o^2}{H}\right)\frac{\partial^2 \zeta}{\partial x^2} + \left(\frac{3\mu u_o^2}{H^2} - \frac{2i\sigma u_o}{H}\right)\frac{\partial \zeta}{\partial x} + \left(\frac{\sigma^2}{H} + \frac{2i\sigma\mu u_o}{H^2}\right)\zeta = 0 \tag{15}$$

having chosen a time dependence of the form $\zeta(x,t), u(x,t) \leftarrow\rightarrow e^{-i\sigma t}$.

$u_o^2/H \ll g$ in areas where $u_o \leq 1$ m/s and $H \approx 5$–10 m; $2\sigma u_o/H$ is at least ten times smaller than $3\mu u_o^2/H^2$. Neglecting these, the solution of (15) has the form:

$$\zeta = \zeta_o e^{kx - i\sigma t} \tag{16}$$

where:

$$k = -\frac{3\mu u_o^2}{2gH^2} + \frac{i}{2}\left[\left(\frac{4\sigma^2}{gH} - \frac{9\mu^2 u_o^4}{g^2H^4}\right)^2 + \left(\frac{8\sigma\mu u_o}{gH^2}\right)^2\right]^{1/4} \exp\left(\frac{i}{2}\arctan\left[\frac{2\sigma\mu u_o}{\sigma^2 H - \frac{9\mu^2 u_o^4}{4gH^2}}\right]\right) \tag{17}$$

The + sign appears before the second term to ensure damping in the increasing x direction (product $(i)x(i) = -1$). The terms in $\mu^2 u_o^4$ are small but not completely negligible, they arise from oscillations in the height of the water column (shallow water effects). The damping is controlled not only by μ but also by u_o and σ. The relative magnitude of the tidal components has now ceased to matter, the outgoing current $-u_o$ is the only portion of the current participating in the damping. The damping is frequency dependent, thus the components will not fade at the same rate, those with the lowest frequencies reaching further upstream. The phase increase is also frequency dependent, so that each component travels at its own velocity. One may compare solution (16) where k is given explicitly in (17), with the formula:

$$\zeta = \zeta_o e^{[-rx - i(\sigma t - rx)]} \tag{18}$$

where $R = \frac{1}{H}\sqrt{\frac{\sigma\mu u_o}{g}}$, u_o being the current due to the fresh water discharge Q. ζ_o is the tidal amplitude at the mouth of the river (Leblond, 1978). The symbol r in the formula controls the damping and the phase increase, implying that if the amplitude varies, so should the phase. The more complete solution (16) (17) indicates additional damping amplitude caused by shallow water effects which leave the phases unaffected. In areas of shallows, the current u_o becomes large so that the ratio u_o^2/gH no longer is negligible. Solution (18) in this zone becomes:

$$k \approx -\frac{3\mu u_o^2}{2g'H^2}\left[1 + \sqrt{1 - \frac{8g'H^2\sigma}{9\mu u_o^3}}\,i\right] \qquad (19)$$

where $g' = g - u_o^2/gH$; the discrepancy in the rates of damping and in the speed of progress of the wave becomes even more marked.

The Saint Lawrence system

The Saint Lawrence systems consists of a wide and deep estuary, the bed of the river becoming narrower and shallower as one moves upstream. The narrowest point lies in the vicinity of Québec Bridge, the river continuing towards Montréal in a bed of varying width but near constant depth. The tides exhibit an oceanic character in the estuary but eventually become distorted past the constriction at Pointe des Monts. The tides, however, continue to increase in amplitude until Ile aux Coudres. Beyond this point, the signal weakens and becomes extinguished past Lake St. Peter. However, during intervals of strong tides, an indication of a tide (1–3 cm) can be sensed at Sorel. Associated with the distortion, long period (15 and 28 days) waves are created upstream having an amplitude of some 30 cm at Grondines. Being of low frequency they are little attenuated; at Trois Rivières they may exceed by a factor of three the oceanic tide reaching the town. The waves still amount to some 20–25 cm at Sorel, while at Montréal they are the only type of tides which may be detected. To proceed with numerical studies on the tidal propagation, hydrographic charts were used to divide the river bed into 53 segments of approximately constant width and depth (and perforce of varying length) (Godin, 1971), from Pointe des Monts to King Edward Pier, some 658 km. The segment Québec–Montréal consists of a regular channel some 200 km long, running along the Logan fault, uncluttered by sediments from the Great Lakes which were shed in the Thousand Islands area,

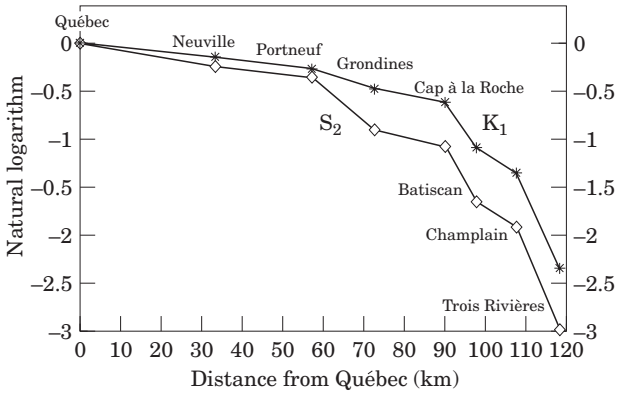

FIGURE 14. Decay profiles of the diurnal and semidiurnal harmonics K_1 and S_2 in the upper reaches of the Saint Lawrence river. K_1 being of lower frequency than S_2 decays less rapidly than S_2.

thus supplying us with the perfect field laboratory for testing our hypotheses. The tidal records in the upper Saint Lawrence cover approximately the years 1964–1979; digitization was introduced then and the gauges worked perfectly and almost continuously for years on end. Additional gauges between Sorel and Montréal were maintained in the 1960's. The network was allowed to disintegrate later on, but what remains is a treasure trove for scientific studies, especially since it virtually has never been examined.

Profile of the tidal harmonics in the Upper Saint Lawrence River

The stations for which annual harmonic analyses exist are listed in Figure 14. We repeat the caveat expressed when inspecting Figure 3: the concept of harmonic ' constants ' cannot be maintained in the presence of quadratic friction. What an analysis provides, is mean values around which the components oscillate during the course of the year (at least those well separated from the others); however the averages vary little from year-to-year for the major components. So we continue to examine these, since they still supply some relevant information. Figure 14 shows the logarithm of the ratio of the amplitudes upstream to that found at Québec, for the components K_1 and S_2 while Figure 15 displays their speed of progress from Québec. Since the components have widely differing frequencies (15° and 30°/h) they do diverge: S_2 is more damped and travels more rapidly. We attempt in Figures 16 and 17 to verify this divergence within a frequency band. O_1 has a frequency of 13·9°/h, N_2 28·4°/h, both less than K_1 and S_2, so it is indeed the case. In Figure 18 we observe the profiles of the amplitudes for M_2 and N_2. M_2, being the dominant

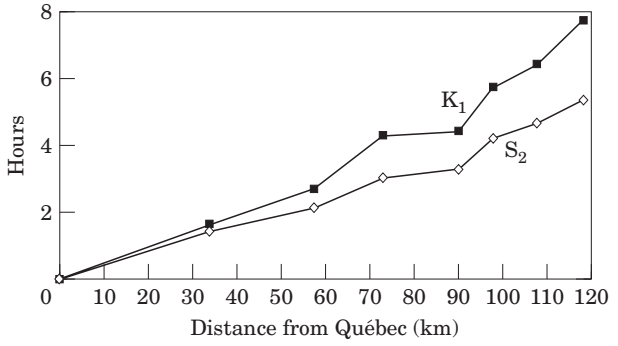

FIGURE 15. Rate of progress, shown in hours, required to reach the site from Québec, of the components K_1 and S_2 in the same area. Due to the lower frequency of K_1, its speed is lower.

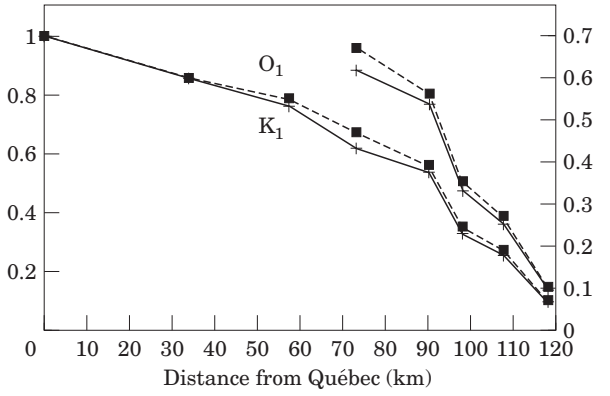

FIGURE 16. Decay profile of the diurnal harmonics O_1 and K_1, which are much closer in frequency; yet the discrepancy in their decay rate is still obvious.

harmonic, should be less damped than its companions. Although it has a higher frequency, its damping is less than that of N_2 as far as Grondines; it results in fact, that its rate of decay is less than that of the others, regardless of their frequency. We did not show these in the diagram to avoid clutter. Beyond Grondines however, there exists a point where u_o becomes the predominant contributor to friction, M_2 then begins to behave as the other harmonics.

Estimate of the friction coefficient μ

We use the stations located between Montréal and Sorel where there are virtually no oceanic tides left, to seek a value for μ. A plot of the position of the river surface, as revealed by the local gauges, shows that its slope is virtually an invariant ($\approx 2{\cdot}6 \times 10^{-5}$), whatever the value of the discharge Q. Chézy's constant C being determined by the current u_o and the surface slope:

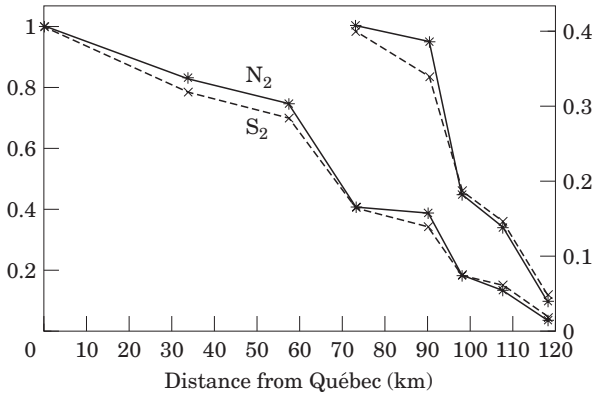

FIGURE 17. Decay profile of the semidiurnal harmonics N_2 and S_2, rather well separated in frequency. Their decay rates are quite distinct over a good portion of the river.

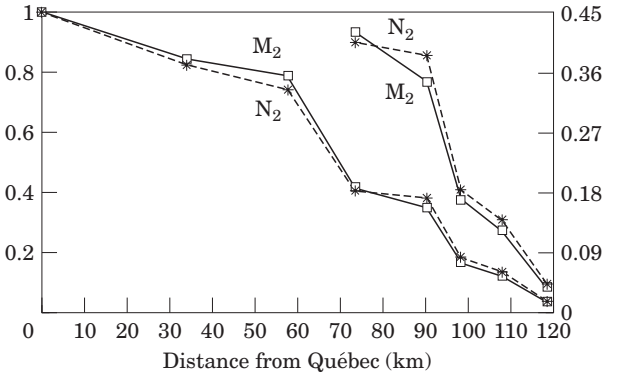

FIGURE 18. Decay profile of the semidiurnal harmonics M_2 and N_2. Quadratic friction and the large size of M_2 cause N_2 to be more damped than its dominant companion initially. Beyond Cap à la Roche, however, the fresh water discharge Q becomes the preponderant contributor to friction so that the higher frequency of M_2 and the quadratic law of friction cause it to be more damped than N_2.

$$u_o = C\sqrt{H_o \frac{dH_o}{dx}} \qquad C = \frac{u_o}{\sqrt{H_o \dfrac{dH_o}{dx}}} \tag{20}$$

In terms of the discharge Q and the river width W:

$$C = \frac{Q}{W\sqrt{H^3 \dfrac{dH}{dx}}}$$

A plot of Q against $H^{3/2}$ gives a near constant value of 483 $m^{3/2}/s$ for $Q_o/H^{3/2}$, for all of the stations between Montréal and Sorel (King Edward, Frontenac, Lavaltrie and Lanoraie); since the mean width of the segment is 1800 m, we get $C \approx 53\ m^{1/2}/s$. That portion of the river thus supplies the estimate:

TABLE 2. Application of solution (16) (with (17)) to three portions of the upper Saint Lawrence River

Channel	Wave number (10^{-2}/km)			
	Diurnals		Semi-diurnals	
	phase	damping	phase	damping
Québec–Portneuf L=57·3 km u_o=0·36 m/s H=11·8 m	0·947	− 0·775	1·471	− 0·957
Portneuf–Cap à la Roche L=33·1 km u_o=0·81 m/s H=6·53 m	1·303	− 2·013	3·487	− 3·739
Cap à La Roche–Trois Rivières L=28 km u_o=0·68 m/s H=5·8 m	2·406	− 2·942	3·563	− 3·646

The value of u_o is based on the assumed mean value of Q=8 550 m^3 s over the years, 1955–92.

$$\mu = \frac{9}{C^2} = 3{\cdot}49 \times 10^{-3} \qquad (20A)$$

With this value and the schematization of the river bed, we have enough information to estimate from formula (17) the theoretical rates of decay and the phase velocities. Figures 14–18 suggest that between Québec and Trois-Rivières, we encounter three zones; Québec to Portneuf, Portneuf to Cap à la Roche, and Cap à la Roche to Trois-Rivières. Table 2 shows the average width and depth for the three channels, and the estimate values. u_o is based on the mean of all the means of Q between the years 1955–1992, which is 8550 m^3/s. The minimum Q occurred in 1964 (6410 m^3/s), the maximum (14 700 m^3/s) in 1973. Figure 19 shows a comparison between the observed ratios and the fits for the diurnals. The model overestimates the damping in the first two channels, while it underestimates it in the third one (the same result for the semi-diurnals). The values obtained are based on a drastic averaging of the channel features. From these values it can be concluded that if a numerical agreement is to be sought, a much more careful schematization of the river bed should be performed. Such an arduous undertaking becomes necessary only when the consequences of vast engineering projects need to be considered (Dronkers, 1964), we should be satisfied that we reached, at least, qualitative agreement between the basic theory and observations.

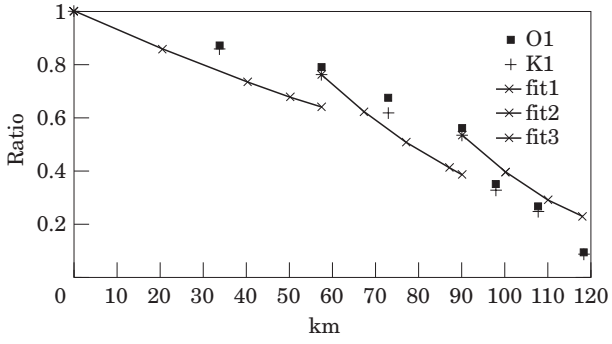

FIGURE 19. Damping profile for O_1 and K_1, using the damping coefficients in Table 2 to verify the effectiveness of solution (16) (with (17)) to represent the decay (far from successful).

The compound harmonics

So far we considered only the original harmonics. If we wish to study the new harmonics created by the non-linear interactions, one approximates the non-linear terms by using the linear solutions for the incoming harmonics, the set of improved solutions being calculated iteratively. Since the incoming harmonics vary with time, the task rapidly becomes formidable. It is more useful to scrutinize the observations themselves to evaluate the distortion of the signal as it actually occurs.

We start with the low frequency compound harmonics (they arise from the term $\sigma_i - \sigma_j$ in Table 1), which are associated with the interference cycles of M_2 and S_2 (MS_o=14·77 days), M_2 and N_2 (MN_o=27·55 days) and K_1 and O_1(KO_o=13·66

TABLE 3. Resulting amplitude of a signal of amplitude 1 m over the relevant periodicities after filtering through the tidal eliminator

Period days	Amplitude after low passing cm
∞	100
$27{\cdot}6 = MN_o$	99·32
$14{\cdot}8 = MS_o$	97·64
$0{\cdot}997 = K_1$	00·00
$0{\cdot}518 = M_2$	00·00
$0{\cdot}500 = S_2$	00·00

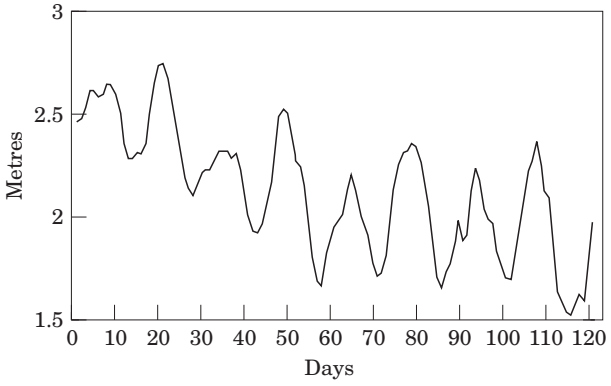

FIGURE 20. Low pass of the hourly values of the water level recorded at Grondines over the interval July–October 1974; the intent is to remove the tidal signal and to retain the slow periodicities.

days). We have to place MS_o and KO_o together since they cannot be separated in a noisy signal. Figure 20 reveals the low pass of the hourly values of the water level at Grondines which was obtained by applying the tidal eliminator (Godin, 1972):

$$\Omega_{24}^2 \quad \Omega_{25}$$

To obtain Ω_n, the mean over n consecutive hours is calculated and a power indicates the number of times that it is applied. This filter was evaluated by Thomson (1983) who found it to be the best three-day filter next to the optimum filter. Table 3 lists the resulting amplitude of a white signal of amplitude 1 m: the original tides are completely cut off while the signal of interest is allowed through almost intact. Figure 20 indicates that the local level is maintained by both Q and the neap-spring cycles. Figure 21 shows a least square fit to the low pass using R, the local tidal range, and Q at Montréal. The calculation was performed for Québec; this time for the entire year (Figures 22 and 23), note the storm surges at the end of the year. What

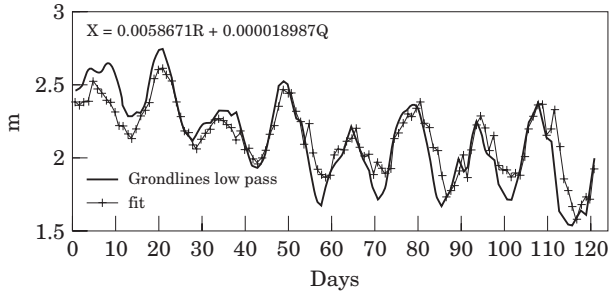

FIGURE 21. Fit of the low pass by the linear model $X = \alpha R + \beta Q$. R is the local range of tide (difference in height between HW and the following LW), Q is the fresh water discharge measured at the entrance of Saint Lawrence Seaway.

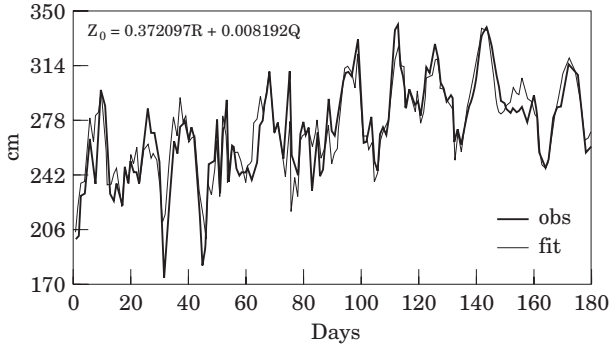

FIGURE 22. Same type of fit for the first half of 1974 for Québec. R this time being the range observed at Québec.

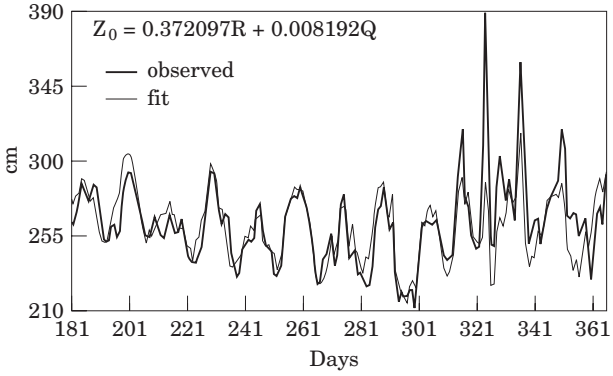

FIGURE 23. Fit for the latter half of 1974 using the same fitting parameters.

we see are the MS_o,MN_o,KO_o mentioned. The model can predict the long period fluctuations in level which are important upstream of Québec.

The high frequency harmonics (associated with $2\sigma_j$, $\sigma_j+\sigma_k$, $3\sigma_j$, $\sigma_j+\sigma_k+\sigma_n$ in Table 1) distort the profile of the wave; the double frequencies are the most

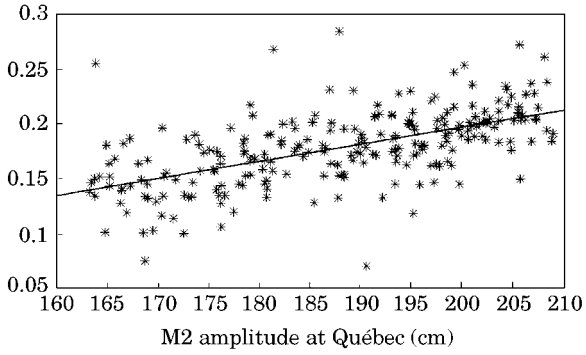

FIGURE 24. Plot of M_4/M_2 at Québec against the corresponding M_2 amplitude; M_4 being created by non-linear effects becomes larger as the local M_2 increases.

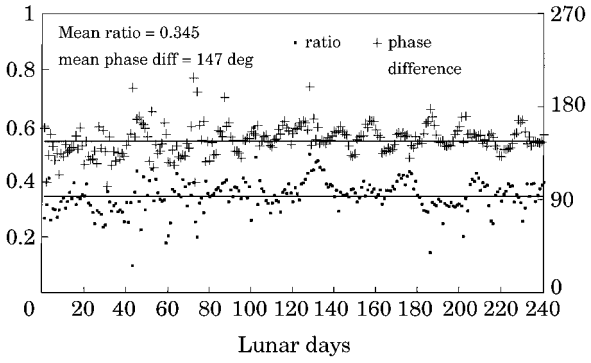

FIGURE 25. Ratio of M_4 at Québec to the M_2 amplitude at Sept Iles. The uniform relation indicates that M_2 at Sept Iles should be the parameter used to predict M_4 at Québec.

important. To investigate these we use the concept of 'reduced vector' introduced by George and Simon (1984). This is obtained by extracting from 25 hourly samples band estimates of the major tidal components. As the samples are made over time they are modulated by the aliased frequencies. This makes the range of variation quite wide during the course of one year. We consider only the M_2 and M_4 reduced vectors. The scrutiny of their variation, from sample-to-sample, also helps detect the occurrences of short term irregularities, a very useful feature.

Since the wave is distorted non-linearly as it progresses from Sept Iles into the river, the relation in amplitude and phase between M_4 and M_2 cannot remain constant. We verify this in Figure 24 where the amplitude ratio M_4/M_2 at Québec as a function of the local M_2 amplitude is plotted. The relative amplitude of M_4 varies from 0·14–0·22 between extreme values of M_2, disregarding the noise. In contrast, Figure 25 shows the amplitude ratio and the phase relation between the M_2 introduced at Sept Iles, and the M_4 sensed at Québec during the year. In this case, the mean amplitude ratio is 0·345, with an average phase difference of 147°. The M_4 M_2 phase difference is defined by $2g(M_2) - g(M_4)$, g denoting the Greenwich phase lag. The physical origin of the quarter diurnals is the steepening of the front of the advancing tidal wave as it meets the outflow of fresh water, shortening the interval of rising levels and lengthening the ebb. Figure 26 illustrates a comparison between the amplitude and phase of the local M_4 at Québec, and those estimates from reduced M_2 vector samples at Sept Iles and 25 hourly values of Q as input, to reproduce the observed M_4 at Québec. The model is:

$$X_4(\text{Qué}) = A[X_2(\text{SI})]^2 + Q(\text{Lasalle})\frac{[X_2(\text{SI})]^2}{|X_2(\text{SI})|^2} \quad (21)$$

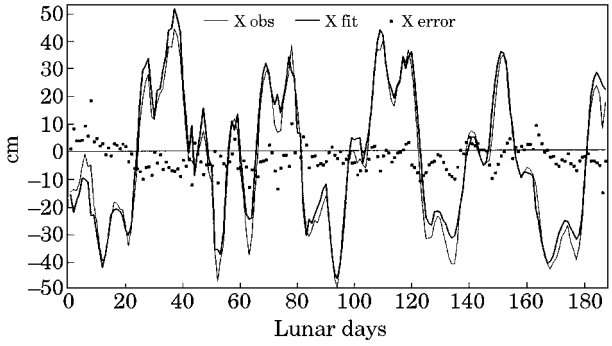

FIGURE 26. Fit of the x component of the M_4 amplitude at Québec from the M_2 sensed at Sept Iles and the value of Q at Lasalle using model (21), to illustrate the effectiveness of the model. Statistical models are generally more successful than physical models, as confirmed by Figure 19.

X indicates the reduced vector with its index. For a least square fit:

$$\Sigma_i X_4(i)\frac{[X_2^*(i)]^2}{|X_2(i)|} = \Phi\Sigma_i|X_2(i)|^2 + \Psi\Sigma_i Q(i)|X_2(i)| \quad (22)$$

$$\Sigma_i X_4(i)\frac{Q(i)[X_2^*(i)]^2}{|X_2^*(i)|^2} = \Phi\Sigma_i Q(i)|X_2(i)| + \Psi\Sigma_i Q(i)^2 \quad (23)$$

Φ and Ψ are the complex coefficients to be determined, the products on the right are found to be real. The terms:

$$\frac{X_2^2}{|X_2|} \quad Q\frac{X_2^2}{|X_2|^2}$$

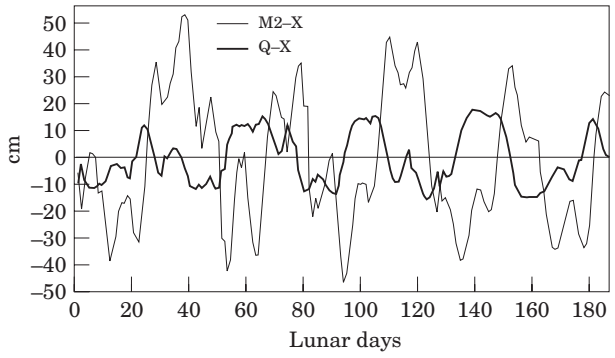

FIGURE 27. Individual contributions of the M_2 at Sept Iles and Q at Montréal to the M_4 at Québec. The fluctuations in the freshwater discharge at Montréal are quite relevant to the value of M_4 sensed at Québec.

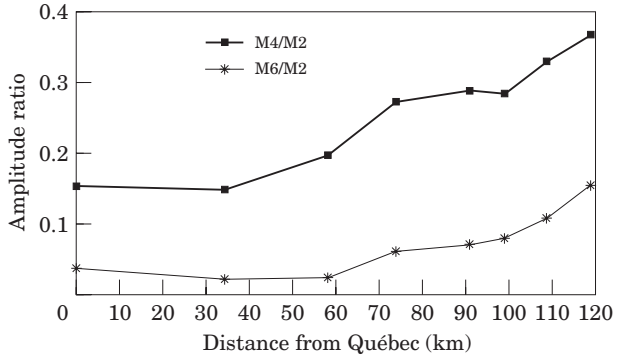

FIGURE 28. Ratios of amplitudes M_4/M_2 and M_6/M_2 past Québec.

were used to double the frequency of M_2 and to introduce M_4 oscillations in Q which is a slowly varying function. For the year 1974, X_2 at Sept Iles and Q at Montréal give:

$$\Phi = (-0{\cdot}199852, -0{\cdot}291117)$$
$$\Psi = (-0{\cdot}846012, 1{\cdot}004506)$$

with units Q–Q/10 000 X_2–X_2 X_4–X_4. The M_2 and M_4 components reaching Québec are generated by the M_2 at Sept Iles, some of the M_2 energy being used to create M_4. From a physical point of view M_4 cannot exist without Q. It becomes of interest to verify in model (21) how much Q (or more precisely, its fluctuations) contributes to the local M_4. We show in Figure 27 the individual contributions of the two terms to the x component of M_4 when, as a complex number, it is expressed in cartesian co-ordinates (x,y) in Equation (21). Without doubt M_2 predominates but the fluctuations in Q are far from negligible. In particular, if we verify around day 140, Q adjusts the estimated x value to fall nearer the observed x. Figure 26 makes this explicit, it shows as points the net difference between the observed x and the fit, which is now transformed into a nearly perfect white noise.

As one moves beyond Québec (Figure 28) the relative importance of M_4 increases steadily.

Biases in HW and LW height and time

HW occurs some time after the flood current starts running while LW follows the ebb current. Equation (1) indicates that these do not coincide with the peak currents, but that they follow them:

$$\mathrm{HW} \leftrightarrow u = +|u|$$

$$\frac{\partial u}{\partial t} = -g\frac{\partial \zeta}{\partial x} - \mu\frac{u^2}{H+\zeta};\ \mathrm{LW} \leftrightarrow u = -|u|$$

$$\frac{\partial u}{\partial t} = -g\frac{\partial \zeta}{\partial x} + \mu\frac{u^2}{H-\zeta}$$

The flood current has therefore started to fall rapidly when HW occurs; the ebb current however, is weakening but not as sharply, at the moment of LW. Harmonic analyses for Québec reveal the phase relation $2g(M_2) - g(M_4) = 90°$; their superposition $\cos\sigma t - a\sin(2\sigma t)$ where $a = 0{\cdot}20$ results in the following:

M_2 alone: extrema $= \pm 1$ at $\sigma t = 0, 180°$;
$M_2 + M_4$: extrema $= \pm 1{\cdot}07$ at $\sigma t = -19°, 199°$

which is exactly the behaviour of HW and LW depicted in Figures 12 and 13.

Effect of the fresh water discharge on the incoming tide

The second line in Table 1 indicates that the immediate effect of the freshwater discharge on the incoming tide is dampening. If Q increases, the wave will not reach as far into the river. Figure 29 shows annual samples of M_2 at Grondines, these correlating negatively with Q; this implies that past Québec, Q controls the amplitude of the tide. Q also controls the local ranges and the times of arrival of HW and LW. For this purpose we chose, between the years 1970 and 1979, intervals of large, small and intermediate discharge, seeking the corresponding signal downstream, then correlating everything with what occurs

TABLE 4. Effect of variations in the fresh water discharge reflected by the value of the correlation coefficient with increasing discharge

Semi-diurnal signal	Amplitude	Phase	
Québec	corr = − 0·07	corr = − 0·22	
Portneuf	corr = − 0·25	corr = +0·18	
Batiscan	corr = − 0·89	corr = +0·46	
Trois-Rivières	corr = − 0·63	corr = +0·11	
	Range	Time interval for	
		LW	HW
Portneuf	corr = +0·12		
Grondines	corr = − 0·80	corr = +0·51	corr = − 0·18
Batiscan	corr = − 0·81	corr = +0·07	corr = +0·64
Trois-Rivières	corr = − 0·85	corr = − 0·47	corr = +0·17

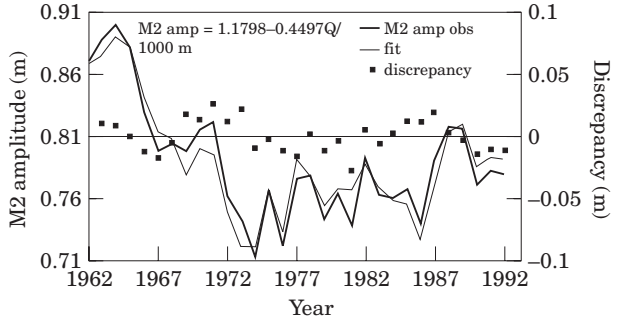

FIGURE 29. Annual values of M_2 at Grondines fitted with Q. Although the presence of M_2 at Grondines is caused by the oceanic tide, its local value is controlled by the freshwater outflow.

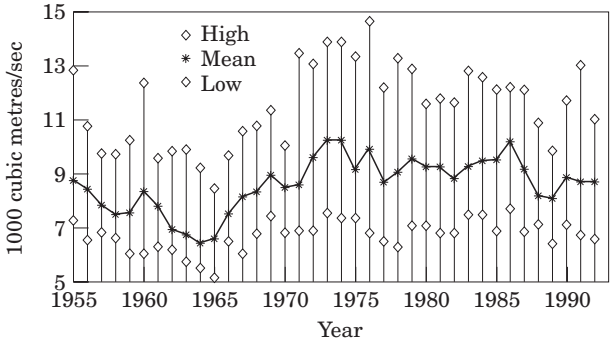

FIGURE 30. Q at Lasalle, means, highest and lowest daily values. The solid lines passing through the stars marks the evolution of the mean annual values. The lozenges mark the largest and the least daily values reached by Q over the course of the year.

upstream. Table 4 lists correlations between such parameters and Q. These are clear for the amplitudes; they are not as marked for the phases reflecting solutions (16) and (17). The speeds of HW and LW become increasingly different past Québec and respond in opposite manners to changes in Q. An increasing Q does enhance the damping past Québec. Finally Q is shown in Figure 30, the solid line marks the mean yearly value. The two lozenges locate the largest and the least daily values that Q passed through during the year. The freshwater outflow from the Great Lakes is carefully controlled. Despite all attempts at control, Q may still vary from factors of three to one over a year. We encounter years of drought (1965, min = 5130 m^3/s), or of excess precipitation (1976, max = 14 600 m^3/s). As a variable, Q can be predicted days, weeks and possibly months in advance, which is the type of information required to improve the tide predictions in the upper regions of rivers.

Effectiveness of tide predictions in rivers

Figures 8 to 11 indicate that tide predictions in rivers are not very successful for the reasons described. Since 1967, the time and height of HW and LW at Québec and Grondines have been predicted using the times of transit of the Moon over Greenwich and the aliased frequencies of the tidal harmonics over intervals of one lunar day (Godin *et al.*, 1967). The programme has not been revised nor updated since: it will also become obsolete by the year 2000 since the times of transit were not calculated beyond the millenium. Errors on the HW time for Québec average to around zero with a standard deviation of 12 min; those on its heights, once corrected for Q, have a standard deviation of 15–25 cm. Errors on LW have systematic components of 12 min and 11 cm. Removing the periodicities does not significantly reduce the standard

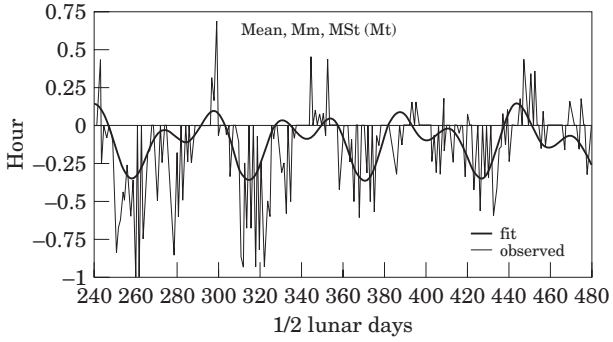

FIGURE 31. HW time error at Grondines, HW starts to show the same type of irregularity as LW (year 1974).

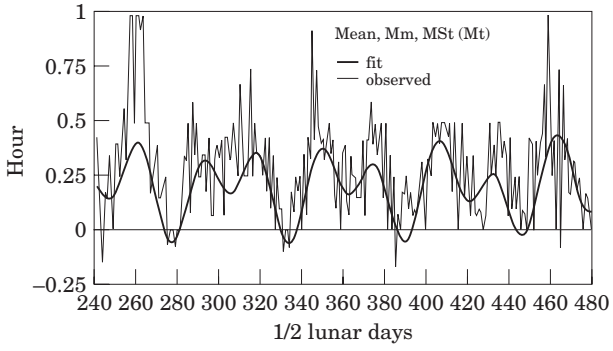

FIGURE 32. LW time error at Grondines, clearly worse than at Québec.

deviations: using the level predicted by Q, or the one from the tables is indifferent. This phenomenon is explained in physical terms by Knight (1981). HW is determined by the incoming tide while the LW marks the point and time when the influence of the tide vanishes, the river simply reaches the level it would maintain in the absence of a tide.

Another site of predictions upstream is Grondines (Figures 31 and 32); systematic errors being now found in both HW and LW, HW occurs earlier and LW later. We presume that matters will become even worse further upstream.

Improved predictions will become possible when more careful consideration is given to fluctuations in Q, implying that short-time predictions should be considered, not conventional tide tables. The instantaneous mean level is also dependent on weather, particularly atmospheric pressure gradients and winds along the river. Finally, what appear as random fluctuations in the errors have, in fact, a definite and deterministic physical origin. In principle these can eventually be identified and quantified by a systematic physical investigation.

Conclusions

Once the tide has penetrated into a river, it is no longer supported by tidal forces. Even if its initial energy can be such that it may generate large tidal ranges and even shock waves, it eventually is wasted away by bottom friction and the braking effect of the fresh water outflow. Modulations in the timing and in the range of the incoming tide reflect the changes occurring in the oceanic tide which is energizing it. Modulations having the same periodicities also displace the position of the mean level around which the oscillations take place. The first effect originates from the non-linear nature of bottom friction while the second one is caused by the interaction between the wave and the outgoing flow of fresh water. The volume of fresh water retained in the river during spring tides is larger, thus raising its mean level. The periodicities themselves reflect the interference cycles between the major components of the tide, namely 15 days and 1 month. All of these distortions increase in importance as the wave progresses upstream, until a point is reached where it starts to be rapidly extinguished. Due to the pressure of the outgoing flow, HW occurs earlier and LW later, than they would in its absence. The timing and height of LW which coincide with a minimum in energy, will be most easily disturbed by transients such as winds or atmospheric pressure gradients. The rate of extinction of the wave, essentially an exponential decay described in solutions (16), (17) and (19) is, as for all exponential processes, very sensitive to fluctuations in the variables which determine the decay constant and to the presence of extraneous factors. We could progress further in the study of the tide in a specific river, by identifying the important local factors controlling its dynamics and by conducting out carefully planned field experiments.

References

Bendat, J. S. & Piersol, A. G. 1966 *Measurement and Analysis of Random Data*. Wiley, New York, pp. 209-236.

Doodson, A. T. 1924 Perturbations of harmonic constants. *Proceedings of the Royal Society (London)* **A106,** 513–526.

Doodson, A. T. 1956 Tides and storm surges in a long uniform gulf. *Philosophical Transactions of the Royal Society (London)* **A237,** 325–343.

Doodson, A. T. 1957 The analysis and prediction of tides in shallow water. *International Hydrographic Review* **33,** 85–126.

Dronkers, J. J. 1964 *Tidal Computations in Rivers and Coastal Waters*. North-Holland Publishing Co. Amsterdam, 518 pp.

Ekman, V. W. 1953 *Studies on Ocean Currents*. Geophysical Publications. Oslo **19,** 274 pp.

George, K. J. & Simon, B. 1984 The species concordance method of tide prediction in estuaries. *International Hydrographic Review* **61** (1), 121–146.

Godin, G. 1971 Hydrodynamical studies on the St Lawrence river. MS report, No. 18 Marine Sciences Branch. *Energy, Mines and Resources*. Ottawa, v+116 pp.

Godin, G. 1972 *The Analysis of Tides*. University of Toronto Press and Liverpool University Press. Toronto and Buffalo, xxi+264 pp.

Godin, G. 1981 Cotidal charts for Canada. MS Report No. 55 *Fisheries and Oceans*. Ottawa, 93 pp.

Godin, G. 1991*a* Compact approximations to the bottom friction term for the study of tides propagating in channels. *Continental Shelf Research* **11** (7), 579–589.

Godin, G. 1991*b* Frictional Effects in River Tides. In *Tidal Hydrodynamics* (Parker, B. B., eds). John Wiley & Sons, New York, pp. 379–402.

Godin, G. & Martinez, A. 1994 Numerical experiments to investigate the effects of quadratic friction on the propagation of tides in a channel. *Continental Shelf Research* **14** (7/8), 723–748.

Godin, G., Taylor, J. D. & Ewing, S. E. 1967 The analysis of nineteen years of observations on the high and low water with the aid of the German method. MS Report No. 3. *Energy, Mines and Technical resources*, 115 pp.

Jenkins, G. M. & Watts, D. G. 1968 *Spectral Analysis and its Applications*. Holden-Day, San Francisco, 525 pp.

Knight, D. W. 1981 Some field measurements concerned with the behaviour of the resistance coefficients in a tidal channel. *Estuarine and Coastal Shelf Science* **12,** 303–322.

Lanczos, C. 1956 *Applied Analysis*. Prentice-Hall, New York, 539 pp.

Laplace P. S. 1841 Recherches sur quelques points du système du monde. *Oeuvres complètes* **9,** 88–107.

LeBlond, P. H. 1978 On tidal propagation in shallow rivers. *Journal of Geophysical Research* **83,** 4717–4721.

Pingree, R. D. 1983 Spring tide and quadratic friction. *Deep-Sea Research* **30,** 929–944.

Proudman, R. D. 1953 *Dynamical Oceanography*. Methuen, London, xii+409 pp.

Thompson, R. O. R. Y. 1983 Low pass filters to suppress inertial and tidal frequencies. *Journal of Physical Oceanography* **13** (6), 1077–1083.